Available online at www.sciencedirect.com

ScienceDirect

Procedia CIRP 89 (2020) 79–91

www.elsevier.com/locate/procedia

CIRP BioManufacturing Conference 2019

Experimental investigation of biological and mechanical properties of CoCrMo based selective laser melted metamaterials for bone implant manufacturing

Saiful Anwar Che Ghani[a,*], Siti Rohaida Mohamed[a], Munirah Sha'ban[b], Wan Sharuzi Wan Harun[a], Nor Aida Zuraimi Md Noar[c]

[a] *Human Engineering Group, Faculty of Mechanical and Automotive Engineering Technology, Universiti Malaysia Pahang, 26600 Pekan, Pahang, Malaysia*
[b] *Department of Biomedical Science, Kulliyah of Allied Health Sciences, Internaltional Islamic University Malaysia, Jalan Sultan Ahmad Shah, Bandar Indera Mahkota, 25300 Kuantan, Pahang, Malaysia*
[c] *Department of Mathematic, Faculty of Industrial Sciences & Technology, Universiti Malaysia Pahang, 26300 Gambang, Pahang, Malaysia*

* Corresponding author. Tel.:+609-424 6262; fax: +609-424 6222. E-mail address: anwarcg@ump.edu.my

Abstract

Metamaterials are composed of structural elements and their properties are derived mainly from the inner structure of the elements, rather than the properties of their constituent material. In this study, mechanical and biological properties of metamaterial made by selective laser melted cobalt chrome molybdenum (CoCrMo) were studied. Metamaterials of diamond and square shapes unit cells with 1.5–2.5 mm strut length and 0.4–0.6 mm strut thickness was prepared by layer-by-layer additive manufacturing technique. The metamaterials demonstrated excellent biological property under MTT assay cytotoxicity after 14 days cell cultured. Comparisons of the experimental data between two unit cell types made by compression tests exhibited that the stiffness of square shape is always higher 20% than those of diamond type, nonetheless all the tested materials satisfy the young's modulus of human cancellous bone. Furthermore, the compression tests also resulted in determining both unit cell types with strut thickness 0.6 mm and strut length 1.5 mm to meet the compressive strength of human cortical bone. The tailored metamaterials by modifying the unit cell sizes and shapes of fabricated bone implant can be achieved by using additive manufacturing technique. The design concepts of internal structures by determining the properties of metamaterials demonstrated in this study will be valuable in future biomedical applications.

Keywords: Metamaterials; Mechanical properties; Biological properties; Orthopaedic implants; Additive manufacturing

1. Introduction

Metamaterials are artificially engineered components of periodic or non-periodic structures, often at the microscopic structures to exhibit the properties that are not yet been found in nature and in the constituent materials [1]. The properties of metamaterials are not derived from the properties of the compositional materials but from their rationally designed structures where the precise shape, geometry, size, orientation and arrangement of the periodic unit cells can affect the homogenous manner of metamaterials [2]. In the past decade, metamaterials are mostly found in diversity of electromagnetic microwave [3, 4], radio communication [5, 6], optical [7, 8] and photonic applications [9, 10] by designing metamaterials for split ring resonators [11, 12], optical fibre with negative permeability and permittivity [13] and also materials with negative refractive index optical frequency [14, 15]. Recently, metamaterials have been

10.1016/j.procir.2020.05.122

studied in promising biomedical applications particularly for bone tissue regeneration and orthopaedic implants [16].

The implants are enormously successful in relieving pain and restoring the mobility of the patient's life even though the major drawback is still the immature and unpredictable lifespan of the devices. The implants consists of permanent and temporary devices that have been used in a broad range of load bearing application such as fracture fixations [17, 18], total joint replacements [19, 20], dynamic stabilizations [21, 22], dental implants [23, 24] and high degree contouring reconstructive devices [25, 26]. The tremendous demands and the dramatic increased as the consequence of revision surgeries in load bearing implants especially in total hip and knee join replacements have been reported [27, 28]. The big numbers of revision surgeries after implantation have attracted the attention in the worldwide surgeon from the past century. Periprosthetic osteolysis and aseptic loosening became due to stress shielding phenomenon, wear debris and lack of osseointegration become the major factors of revision surgeries in metallic load bearing implants [29-31]. In recent years, the development of load bearing implants has motivated the considerable study on how the interaction between mechanical and biological factors can affects the long term success in the orthopaedic surgeries where the concept of metamaterials for lightweight and capability to support and promote the tissue regeneration load bearing implants.

To date, researchers have shown an increased interest in employing advance additive manufacturing to produce orthopaedic implants with the tailored mechanical stiffness and provide accommodation for human cells to grow and integrated with implants devices naturally [32-35]. Additive manufacturing is the extension of rapid prototyping that used additive method fundamentally layer by layer fabrication technique directly from the information that obtained from a three dimensional computer aided design (CAD) [36, 37]. Additive manufacturing has possible to produce almost reliable design of microarchitecture to achieve the desired set of physical, mechanical and biological properties referring to ideal load bearing implants with patients specific elements [38]. Meta-biomaterials is best to mention when aimed for biomedical applications. The metamaterials configurations cannot be fully controlled since the majority of the existing manufacturing technologies do not allow or limitations for precise control of the shape type, size and interconnect cellular pore distribution [39, 40]. The requirements with complex shape and fully tiny details making the metamaterials are difficult to manufacture using the conventional process such as space holder and gas foaming methods [41, 42].

Apart from Campoli, et al. [43], the mechanical properties of meta-biomaterials in particularly the stiffness values are comparable to the stiffness of human bone. Some studies have shown the beneficial effects of meta-biomaterials in tailoring mechanical properties [33, 44] and for bone regenerations [45, 46] separately. Little is known about the effectiveness of meta-biomaterials in both feature for reducing the stiffness of metallic biomaterials and promotes the bone regeneration into structures. Furthermore, mechanical properties and structural behaviours of cellular materials play key roles in regulating the overall function of the orthopaedic system [47]. Conventionally fabrication process failed in providing porous components with complex shape and desired porosity with tailored mechanical properties [46, 48] which urged current research to explore the relationship between geometrical design of metamaterials structures particularly in biocompatibility and mechanical properties using additive manufacturing techniques [49-54]. Previous studies reported the porosity 45%-90% are favourable for metallic implants with lower elastic modulus while the pore size range from 200-1000 µm for suited for cell ingrowth [55-59]. Thus the studies on metamaterials with pore size bigger than this range are not being found.

The aim of the paper is to produce metamaterials as a basic structure for load bearing implant device. The physical, mechanical and biotoxicity of SLM-ed CoCrMo metamaterials with different design geometrical parameters (i.e. base shape, strut thickness and strut length) are evaluated and tested to assess the compatibility of the design for use as the material of load bearing bone implant. The effect of each test parameter in mechanical and biological properties is significant to tailoring by modifying the internal architectures of the orthopaedic implant device.

2. Materials and methodology

2.1. Materials design and manufacturing process

The medical graded CoCrMo powder with 90% of the powder particle size ranged is 22 µm was used in this study. The powders were nearly spherical shape with smooth surfaces and narrowly distributed which beneficial to additive manufacturing process due to good flowability. The unit cells used as the microarchitecture of the metamaterials namely square and diamond as in Fig. 1. The unit cell lengths were varied from 1.5 mm to 2.5 mm and strut size were varied from 0.4 mm to 0.6 mm which resulted in volume porosity ranging from 45% to 88%.

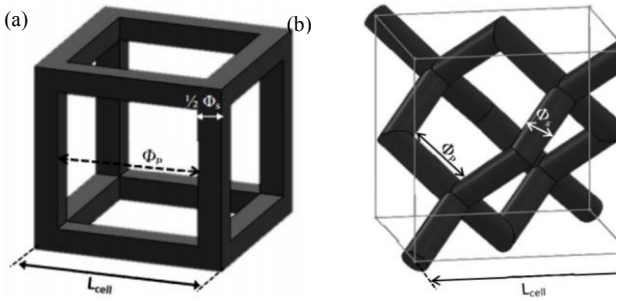

Fig. 1. CAD model (a) square; (b) diamond unit cell type

Table 1 presents the details of geometrical parameters for designed metamaterials. Strut length, strut size and pore size are represented by Lcell, Φ_S and Φ_P, respectively. All geometrical parameters are in mm scale and as a result 10 variations corresponding to five of square shape unit cells and five of diamond shape unit cells will be investigated. Full

dense sample will also be produced as a control.

Table 1. Geometrical parameters of designed metamaterials.

Unit cell type	Sample	Strut length, L_{cell} (mm)	Strut size, Φ_S (mm)	Pore size, Φ_P (mm)
Square	S1	1.5	0.4	1.1
	S2	1.5	0.6	0.9
	S3	2	0.5	1.5
	S4	2.5	0.4	2.1
	S5	2.5	0.6	1.9
Diamond	D1	1.5	0.4	0.9
	D2	1.5	0.6	0.7
	D3	2	0.5	1.2
	D4	2.5	0.4	1.7
	D5	2.5	0.6	1.5

The metamaterials were manufactured using selective laser melting with default parameters as summarized in Table 2 with energy density calculated by using Equation 1. Rectangular metamaterials were manufactured for physical evaluation and mechanical properties with the dimension of 12×12×15 mm. Meanwhile, the samples for biocompatibility testing were manufactured with the dimension 6×6×5 mm. The fabrication process was performed in an inert atmosphere and the metamaterials were built on top of stainless steel substrate. After the fabrication process, the metamaterials were detached from the substrate plate using wire electro discharge machining.

Table 2. Process parameters of selective laser melting.

Parameter	Description
Laser power (W)	300
Laser scan speed (mm/s)	700
Hatch spacing (mm)	0.12
Layer thickness (μm)	30
Energy density (J/mm^3)	119.05
Chamber atmosphere	Argon

$$Energy\ density = \frac{Laser\ power}{Scan\ speed \times hatch\ space \times layer\ thickness} \quad (1)$$

2.2. Physical properties evaluations

The porosity of every metamaterials is calculated according to Equation 2 and 3.

$$\phi = V_P / V_B \quad (2)$$

$$V_P = V_B - V_S \quad (3)$$

Where, ϕ is porosity, V_p is volume porous, V_B is volume bulk and V_S is volume solid.

The density of the metamaterials was measured according to Archimedes principle. The calculation of density and relative density were according to Equation 4 and Equation 5, where the density of water, 1 g/cm^3. The theoretical density was taken as 8.29 g/cm^3 the density of CoCrMo alloy according to standard material specification [60]. Full dense samples with the same dimensional features were used to justify the density measurement of the metamaterials.

$$Density,\ \rho = \frac{Water\ density \times mass\ in\ air}{Mass\ in\ air \times mass\ in\ water} \quad (4)$$

$$Relative\ density,\ \% = \frac{Measured\ density}{Theoretical\ density} \quad (5)$$

An optical microscope (Dino-lite Digital Microscope) was used to investigate and analyses the manufacturability of strut size, pore size and dimensional accuracy of produced metamaterials. The dimensional accuracy (print tolerance) determined the derivation of the finished model by comparing the dimensions to the measurement of CAD model. For every measurement, ten dimensional values were measured at the random points and the average values were calculated.

2.3. Mechanical testing

Quasi-static mechanical properties of produced CoCrMo metamaterials were analysed by compression testing. Prior to the compression test, the metamaterials were subjected to heat treatment in an argon atmosphere at temperature of 1050 °C for two hours for stress relieved and allowing partially melted powder on the struts fused and bonded on the strut core. All produced metamaterials have undergone uniaxial compression test until the mechanical failure occurred. The compression test was performed at constant speed of 0.1 m/min with load of 100 kN using AGS-X series compression tester (Shimadzu, Japan) under normal atmospheric conditions and replication number of n=5 as summarised in Table 3.

Table 3. Mechanical properties testing parameters.

Equipment	Load, kN	Speed rate, mm/min	Replication number, *n*
Shimadzu AGS-X	100	0.1	5

The samples were loaded until failure occurred. The stress stain curve for each individual component was calculated and generated from the real-time force versus displacement data obtained. The following values deviated from the compression test; (1) the elastic modulus as the slope of the compression stress-strain curve in the linear elastic region, (2) the compressive strength calculated by dividing the

highest load by the support before the first fracture in force has occurred and (3) the compressive strain as the corresponding strain at the point of compressive strength. The testing set up was designed and performed in accordance with standard ISO 13314:2011 [61].

2.4. In-vitro biocompatibility

Prior to biocompatibility analysis, all metamaterials were assigned to two experimental groups where the metamaterials were sterilized using different method (1) autoclave with the temperature range from 105°C to 135°C and (2) gamma irradiation ray with exposure dose 25 kGy. Biocompatibility testing was performed of an in vitro cytotoxicity test according to ISO 10993-5:2009 standard [62].

2.4.1. Cartilage harvesting, chondrocytes cell isolation and culture expansion

The Articular cartilage was aseptically dissected from femoral condyles and patellae of an adult rabbit. The animal operation was performed under standard guideline approved by the IIUM Research Ethics Committee (IREC) (reference number: IIUM/305/2014/10). The specimen was washed with phosphate buffered saline (PBS, pH 7.2) (Gibco, USA) containing 100 µg/ml penicillin and 100 µg/ml streptomycin. The specimen was then minced into small fragments and digested with 0.6% collagenase A at 37°C for 4 hours in an orbital incubator at 250 rpm for chondrocytes isolation. After final centrifugation, the cell pellet was washed and resuspended in PBS solution to remove the remaining enzyme and for total cells count. Chondrocyte suspension was treated and evaluated for cell viability using Trypan Blue dye (Gibco, Invitrogen, USA).

Harvested chondrocytes were plated with the initial seeding of 5000 cells/cm^2 in 6-wells plate (Thermo Scientific, Nuclon Delta Surface, Denmark) and cultured in nutrient mixture (F12) and Dulbecco's Modified Eagle Medium (DMEM) (Gibco) supplemented with 10% foetal bovine serum and presence of ascorbic acid, L-glutamine, antibiotics and antimycotic. All cultures were maintained in a standard culture condition of 37°C and 5% humidified CO_2. The primary culture was subcultured until passage 1 (P1) with the medium change every 2 days.

2.4.2. Three dimensional (3D) cell seeding construct

The harvested chondrocytes cells by trypsinization were counted for total cell and viability using haemocytometer (Silverlite, Rohem Instruments, India). Approximately, 100 000 cells per sample were incorporated and resuspended in the culture medium for cell seeding. Cell suspensions in culture medium were seeded directly into each sample and were allowed to soak in an orbital incubator at 130 rpm, 37°C for 5 minutes. After soaking, all constructs were removed and placed into pre-wetted 24-wells plate for incubation in 5% CO_2 humidity at 37°C with the medium changed every day. All constructs were cultured for a maximum of 21 days in-vitro in which the constructs were evaluated at day14 and day 21.

2.4.3. MTT assay cytotoxicity

The cell viability of two experimental groups was measured in vitro by using 3-(4,5-dimethylthiazole-2-yl)-2,5- diphenyltetrazolium-bromide (MTT) (Merck, Merck KGaA, Germany) that measured the reduction of colourless salt tetrazolium by mitochondrial and cytoplasmic dehydrogenases of living metabolically active cells through the formation of intracellular water-insoluble purple crystals of formazan. All constructs were transferred into Eppendorf tube (Eppendorf, Eppendorf Ag, Germany) with 1 ml of new medium. 100 µl of MTT solution (0.5 mg/ml in PBS) was added to all Eppendorf tubes and incubated for 4 hours at 37°C. Then, all constructs were transferred into other new tubes and 1 ml per scaffold of dimethylsulfoxide (DMSO, Merck, Germany) was added to solubilize the resulted crystal. 100 µl of solubilised mixture was then pipetted into a 96-well microtiter plates (Nunclon TM Delta Surface, NUNC, Denmark) and the duplicate readings were recorded by using ELISA plate reader (Versamax Microplate Reader, Molecular Devices, USA) at 570 nm—yielding absorbance as the function of viable cell number.

2.4.4. SEM observations of cell-containing surfaces

To prepare the specimens for morphology analysis under scanning electron microscope (SEM), the constructs were fixed and dehydrated. The samples were washed three times in PBS solution and fixed with sterile 4% paraformaldehyde (Sigma) for 1 hour. After fixation, the samples were rinsed again three times with PBS and subsequently dehydrated in a graded series of ethanol (30%, 50%, 70%, 90% and 100%) every three times for 10 minutes for each wash. All constructs were placed in freezer and freeze-dried for 24 hours using freeze dryer to remove any remaining solvent before observed under SEM.

3. Results and discussion

3.1. Effect of design parameters on physical properties

The variation of controlled unit cell shape *Lcell*, and strut size, Φ_S as in Fig. 1 produced metamaterials with different pore sizes, Φ_P and volume porosity. Generally, it can be observed that for every designed parameter, the resulted pore size and volume porosity of diamond shape unit cells were always smaller than the ones produced of square shape unit cells with designed parameter as in Table 1. The difference in volume porosity of the diamond and square types was in the range of 3-26%. The obtained pore sizes were in homogeneous distribution for both diamond and square types. However, the obtained pore sizes for the square type were consistently about 20% greater than the pore sizes of diamond type metamaterials.

Thus, the correlation between volume porosity and the density including relative density were investigated. The

measured densities of fabricated CoCrMo metamaterials were calculated by using Archimedes principle. Relative density was calculated by the ratio of measured density with specific theoretical material of CoCrMo alloys of 8.29 g/cm^3. Table 4 summarises the measured density and relative density for produced metamaterials including full dense sample for justification.

From the table, the relative densities of metamaterials were varied in the range of 92.49 % to 97.67 % for the square type. Meanwhile, the relative density of the diamond type was varied from 84.68% to 97.29 %. The fully dense samples exhibited relative density of 99.29 %. The good relative density of metamaterials indicated that the produced CoCrMo parts demonstrated the possession of low void on bulk struts which developed as consequences of balling formation and entrapment of gas in melting powder [63]. The influenced of high energy input during the manufacturing process led to higher density of the produced parts. A low percentage of voids in the manufactured parts due to energy density resulted in a higher attained temperature of melted powder and therefore, promote an improved interlayer connection between layers in metamaterials struts [64].

Table 4. Density and relative density of produced CoCrMo metamaterials.

Sample	Porosity (%)	Measured density (g/cm^3)	Relative density (%)
S1	79.8	8.09 ± 0.07	97.67
S2	60.9	7.67 ± 0.45	92.49
S3	81.2	7.92 ± 0.15	95.52
S4	91.0	7.75 ± 0.14	93.48
S5	81.7	7.99 ± 0.17	96.37
D1	70.7	7.02 ± 0.62	84.68
D2	44.8	7.69 ± 0.32	92.70
D3	73.8	7.40 ± 0.39	89.29
D4	88.1	8.07 ± 0.07	97.29
D5	75.6	7.67 ± 0.29	92.57
Full dense	-	8.23 ± 0.01	99.29

The densities of the components have the significant effect on the mechanical properties of metamaterials, whereby the achievement of near fully dense struts is normally expected in SLM fabrication to obtain a strong and high performance of the produced structure as the final outcome [65]. Previously, Yan, et al. [66] found that both relative density and measured density tend to decrease with the increasing of unit cell size and volume porosity. On top of that, Yan, et al. [65] also found that high relative density above 99% was achieved for diamond and gyroid type structures with porosity ranging from 80% to 95%, but the porosity had less effect on the densities of components.

Fig. 2 shows the graph of density and relative density for square and diamond metamaterials in comparison to full dense density. As shown in the graph, the density of square type decreased with the increased of porosity because of less solid struts in the components. However, the density of the diamond type was comparable to the theoretical density of CoCrMo towards the increased porosity. Both square and diamond with unit cell length 1.5 mm and strut size of 0.6 mm exhibited lowest density for each group of metamaterials. This resulted because of excessive partially melted powder and remaining voids on the solid struts. The scan vector lengths could become shorter and the scanning areas become smaller for bigger strut size (0.6 mm). The cross-section area of strut might become smaller in the internal of the metamaterials component. Hence, the adjacent tracks were scanned more swiftly one after the other layer, which left less cool down time in between them that led to higher temperatures of the scanned boundaries [66, 67].

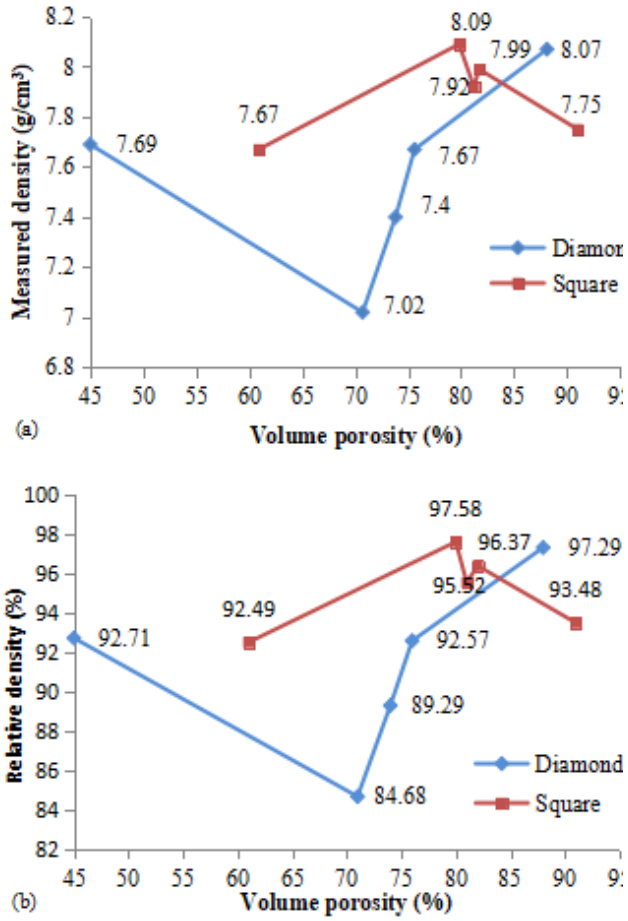

Fig. 2. (a). Measured density (b) relative density of square and diamond unit cell with varied of volume porosities.

Consequently, better wetting conditions were presented to form denser strut in the smaller size (0.4 mm) of struts for both square and diamond unit cell types. Kruth, et al. [68] noted that the processing parameters and scan strategy during the SLM manufacturing process play an important role in producing high density components. Therefore, it is worth carefully investigate the effects of the SLM process parameters and scan strategy on the density of the products in the future works. Furthermore, better density of the metamaterials could be achieved with smaller strut size, while the evaluation using micro-CT images to confirm the cross section on the internal structure of metamaterials can be performed as suggested by Yan, et al. [67] and Pyka, et al. [69].

3.2. Effect of design parameters on manufacturing accuracy

Dimensional accuracy of produced metamaterials was measured to determine the manufacturing accuracy and the shrinkage of SLM-ed products. Dimensional measurements were determined by measuring ten random points and the average value was calculated. The dimensional error was calculated as the absolute different (mm) between the values obtained from the produced metamaterials and the CAD models of each metamaterials design for each linear measurement of the feature length, width, and height [70]. The measurement and calculation of standard deviation and error of accuracy (tolerance) as represented in Table 5. For every square and diamond shape unit cells, five CoCrMo samples with different variations in geometrical parameters have been produced by SLM. A full dense sample of 2,160 mm^3 volume has also been manufactured by the same SLM process as a control.

From the table, the square type (S1) and (S2) mm exhibited shrinkage behaviour on the height dimension. During the SLM process, the short interaction of powder bed and heat source was the resulted of the scanning speed of laser beam that leads to rapid heating and the melting stage [71]. This phenomenon caused the shrinkage of the products. Meanwhile, the square type (S3) obtained the expanded dimensions due to broaden pore which caused the length of unsupported region and the critical overhang dimension became more widen. The melt pool sinks deep underneath the powder and led to the formation of dross on the overhang region as a result of scanning the loose powder of CoCrMo during the manufacturing process. This phenomenon also affects the diamond unit cell type (D1) with respect to their strut angle. It was observed that as the angle approaching the horizontal struts, the strut width also enlarges [72]. There is no significant difference in height dimension accuracy for the rest of the produced diamond type metamaterials.

Fig. 3 demonstrates the highly controlled geometrical parameters metamaterials after the fabrication process. From the figures, the support angle for square type was set to be 45° orientation in order to avoid the overhang in the samples.

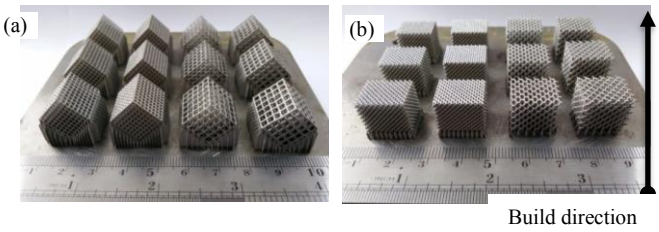

Fig. 3. Produced (a) square and (b) diamond metamaterials on base plate.

Fig. 4 shows the optical microscope images of manufactured metamaterials for both square (S4) and diamond type (D4). In addition, it can be clearly seen that the struts of metamaterials are well fabricated through SLM process because the struts are solid and interconnected despite the rough surface. The surface roughness of SLM products affected by partially melted powder that being attached to the strut surfaces. Geometrical discrepancies and surface roughness associated with partially melted particle have the significant effect on mechanical performance and fracture behaviour [73, 74]. However, it is not a disadvantage for certain implant application criteria such as cell attachment which are enhanced with increased surface roughness [75, 76]. On top of that, the factors of bonded particles on strut have been significantly discussed in numerous researches [77].

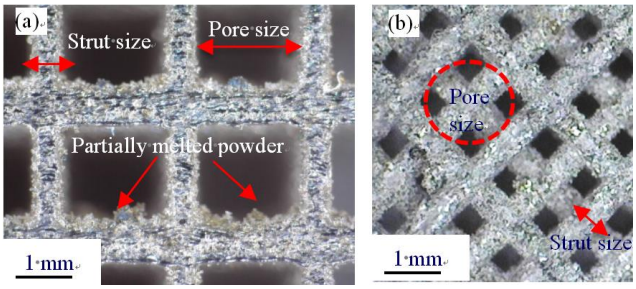

Fig. 4. Morphology of (a) square and (b) diamond.

Table 5. Dimensional measurement of CoCrMo metamaterials.

Sample	Designed dimension ($l \times w \times h$) (mm)	Measured dimension ($l \times w \times h$) (mm)	Standard deviation	Error observation lateral, (l or w) (%)	Error observation vertical, (h) (%)
S1	12.4×12.4×15.4	12.6×12.6×15.3	0.02	-1.61	0.65
S1	12.6×12.6×15.6	12.7×12.8×15.5	0.02	-1.19	0.64
S3	12.5×12.5×16.5	12.7×12.7×16.5	0.05	-1.60	0
S4	12.9×12.9×15.4	13.2×13.2×15.5	0.01	-2.33	-0.65
S5	13.1×13.1×15.6	13.3×13.3×15.6	0.01	-1.53	0
D1	12.0×12.0×15.0	12.1×12.1×15.1	0.01	-0.83	-0.67
D2	12.0×12.0×15.0	12.1×12.1×15.0	0.02	-0.83	0
D3	12.0×12.0×16.0	12.2×12.1×16.0	0.03	-1.67	0
D4	12.5×12.5×15.0	12.7×12.6×15.0	0.05	-1.20	0
D5	12.5×12.5×15.0	12.6×12.6×15.0	0.06	-0.80	0
Full dense	12.0×12.0×15.0	11.9×12.0×15.0	0.06	-0.83	0

The struts were analysed and compared from CAD models to determine the manufacturability of SLM to produce the complex shape of metamaterials as summarised in Table 6. The table presents the designed and actual strut sizes of both square and diamond type. The actual strut sizes for the square type were recorded bigger than designed struts. Meanwhile, produced strut sizes for diamond type exhibited similar from the designed model. The bigger strut size in comparison to the original CAD model was due to remaining partially melted powder particles which are attached to the strut core and melt pool size on the strut boundaries. It is vital to note that the bonded powder particles on the strut surface are caused by two main factors described as follows: (1) the phenomenon of partially melted metal powder particles on the boundary of each layer in the SLM manufacturing process by contour laser track [66], and (2) angle strut are partially solidified on the loose powder due to the big difference in temperature which can cause the powder particles to stick to the strut surface [67, 78]. A similar observation was conducted by Yan, et al. [77] for the purpose of evaluating the strut size of SLM-manufactured 316L stainless steel that was increased by 80 µm using optical microscopic evaluation. Previously, Van Bael, et al. [78] noticed the increase of strut sizes with 122 µm based on the evaluation of SLM-manufactured Ti6Al4V structures conducted through micro-CT image analysis. On the other hand, Parthasarathy, et al. [44] reported the strut size of AM-manufactured Ti6Al4V structures of 140 µm were reduced with a pore size of 210 µm.

Table 6. Manufacturability analysis on strut size of CoCrMo metamaterials.

Sample	Model strut size, Φ_S (mm)	Actual strut size, Φ_S (mm)	Error observation (%)
S1	0.40	0.407± 0.002	-1.82
S2	0.60	0.616± 0.004	-2.75
S3	0.50	0.511± 0.003	-2.10
S4	0.40	0.407± 0.001	-1.40
S5	0.60	0.611± 0.002	-1.88
D1	0.40	0.405± 0.011	-1.12
D2	0.60	0.605± 0.008	-0.78
D3	0.50	0.501± 0.006	-0.12
D4	0.40	0.405± 0.004	-1.15
D5	0.60	0.604± 0.003	-0.60

Good manufacturability of diamond type metamaterials was highly dependent on the build strut angle. Interestingly, the self-supported feature was found to be exhibited in diamond type as a result of the inclination angle between the two adjacent layers, which was believed to be capable of supporting the fabrication of next layer. Therefore, the results of diamond type were in good geometric agreement with the CAD models. However, smaller unit cell size (1.5 mm) of diamond type results was found to be inaccurate due to the loss of connectivity between adjacent cell layers or may be caused by the extremely thin strut features that were initially designed for 0.4 mm and 0.5 mm which interferes with its fabrication by SLM process. Moreover, it is important to notice that the strut angles from the horizontal plane are lower than a certain degree or its overhanging section is beyond a certain length. Hence, deformation tends to occur during fabrication because the struts were mostly built on loose powder which led to the defect of the produced components [79, 80].

3.3. Effect of geometrical properties on mechanical properties of metamaterials

One of the main goals of this study is to obtain the metamaterials with tailored mechanical stiffness with an improved strength to weight ratios in comparison to the human bone properties. The mismatch of stiffness between bone and implant material leads to the inefficient stress distribution which stimulates stress shielding [81, 82] . This phenomena leads to implant failure and finally, revision surgeries are needed. In this present study, CoCrMo metamaterials with different porosity levels were designed, fabricated by SLM and characterized aiming the development of new bone implant solutions to eliminate revision surgeries.

Fig. 5 depicts stress-strain curves of CoCrMo metamaterials. Stress-strain curves were obtained from the experiment where at the early of force loading, the curves had an initial portion that was non-linear and concave upwards which may be the attributed of a small amount of distortion of the struts of metamaterials when it was cut off from the base plate or uneven top or bottom surface. Following it, an elastic region occurred from the stress-strain curve with a relatively high degree of linearity pattern. Following the elastic region, the deformation region occurred where the compression strength can be determined from the curve. Final stage was the fracture or failure which occurred at the higher loading force. The stress-strain curve obtained from this study did not contain the plateau region and densification region which was not similar to the previous studies by [83-85].

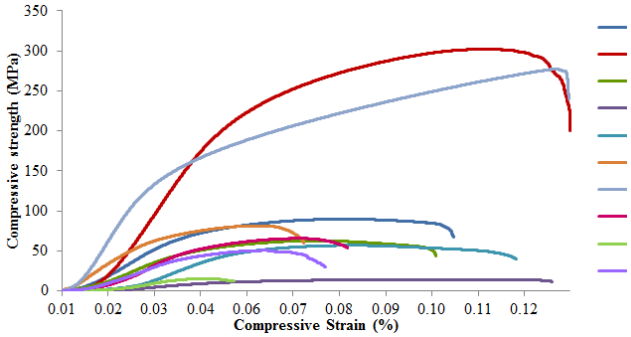

Fig. 5. Stress-strain curves of CoCrMo metamaterials.

Table 7 summarises the results of the compression test that includes elastic modulus, 0.2% yield strength and compression strength. According to the table, the elastic modulus for all designed CoCrMo metamaterials were decreased in elasticity values. The elastic modulus of the metamaterials were within the range of 0.44 and 8.75 GPa.

The values of elastic modulus are comparable with the elastic of human cancellous bone (10 to 15,700 MPa) [86]. However, the ultimate compression strength and compression strength of the full dense sample cannot be obtained due to the limitation of the machine load. Hence, for future works, it is recommended to use the compression tester with higher loading. As expected, the elasticity of CoCrMo can be tailored when the porosity was employed on the bulk components particularly the highly controlled geometrical parameters as in metamaterials structures [87].

Table 7. Mechanical properties of CoCrMo metamaterials.

Sample	Elastic modulus (Gpa)	0.2 % Yield strength (MPa)	Compresion strength (MPa)
S1	4.47 ± 0.67	47.68 ± 0.77	59.97 ± 2.37
S2	8.75 ± 0.12	154.93 ± 1.23	245.03 ± 4.25
S3	2.91 ± 0.66	54.30 ± 1.28	46.67 ± 0.83
S4	0.92 ± 0.09	12.08 ± 1.28	11.81 ± 1.12
S5	2.10 ± 0.05	46.88 ± 2.08	41.10 ± 1.77
D1	2.83 ± 0.21	73.85 ± 2.60	62.93 ± 3.97
D2	7.47 ± 0.08	247.68 ± 1.50	240.08 ± 0.99
D3	2.29 ± 0.09	54.48 ± 2.17	44.59 ± 0.99
D4	0.45 ± 0.02	11.40 ± 0.94	10.77 ± 5.49
D5	1.93 ± 0.10	44.54 ± 1.53	40.04 ± 1.63
Full dense	224.63 ± 0.27	NA	NA

The failure behaviours of metamaterials after maximum load achieved are illustrated in Fig. 6. It was observed that buckling and fracture towards diagonal axis for diamond metamaterials. The cell struts began to bend under compressive loading, and after slight bending, some of the struts experienced brittle fracture. In this case, the deformation or fractures for square type metamaterials where the horizontal shear band at the bottom parts were observed after bending. Meanwhile, fracture in diagonal (45°) shear band of the diamond type metamaterials was observed after buckling in the struts. Previously, the behaviour has been documented similarly by [88-90]. Weißmann, et al. [91] found that the orientation of the unit cell resulted in a change of the mechanical properties of the structures in regard to unit cell length, in which the position of the struts towards the affected force loading and the position of strut angle in building process led to the 45° shear deformation of the twisted type structures. The anisotropic geometries of the structures were important to be considered due to the influenced of the acting forces of the strut on the mechanical properties. The role of cell size and porosity were highly influenced the mechanical behaviour, thus showing a consistent result with [92, 93].

Fig. 7 shows the relationship of the elastic modulus with the porosity of metamaterials. From the figure, the elastic modulus decreased when the porosity increased. However, the high porosity caused drastically decreased of fracture toughness or fatigue resistance of the metamaterials. Thus, desired porosity need to carefully select in order to design metamaterials for bone implant application. A linear correlation between elastic modulus and the porosity was found (R^2= 0.95) for square type metamaterials and (R^2= 0.99) for diamond type metamaterials. Fig. 8 shows the compressive strength value related to the porosity of metamaterials, where the linear correlation of (R^2 = 0.95) for both types of metamaterials were found. Previously, different designed structures following the concept of specific strength has been studied by Yánez, et al. [94], where the structures with orientation angle was discovered to be lower than 35° was found to achieve better specific strength based on the understanding that strength decreases as the angle degree for diamond type increase.

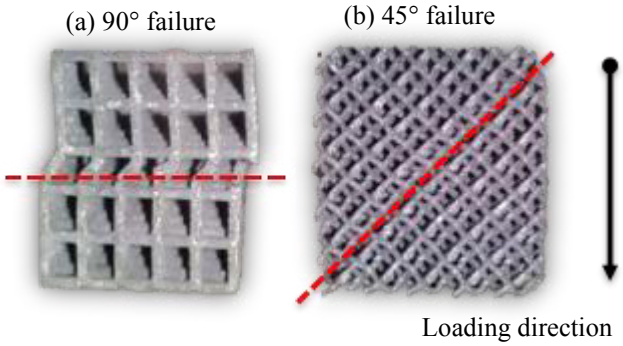

Fig. 6. Failure behaviour of CoCrMo metamaterial (a) square type and (b) diamond type.

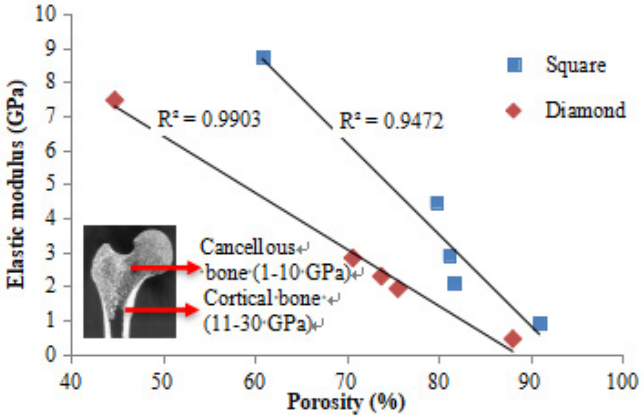

Fig. 7. Relationship of elastic modulus and porosity of the metamaterials.

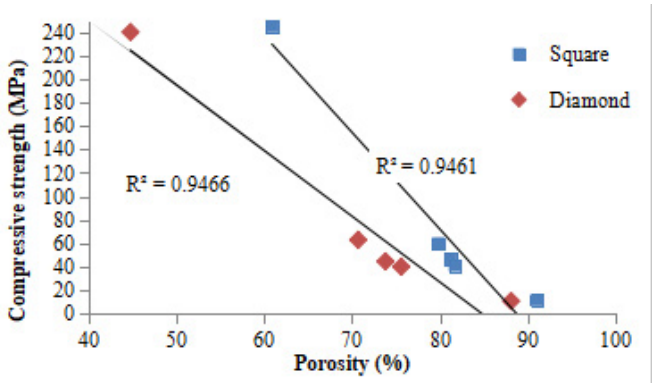

Fig. 8. Relationship of compressive strength and porosity of the metamaterials

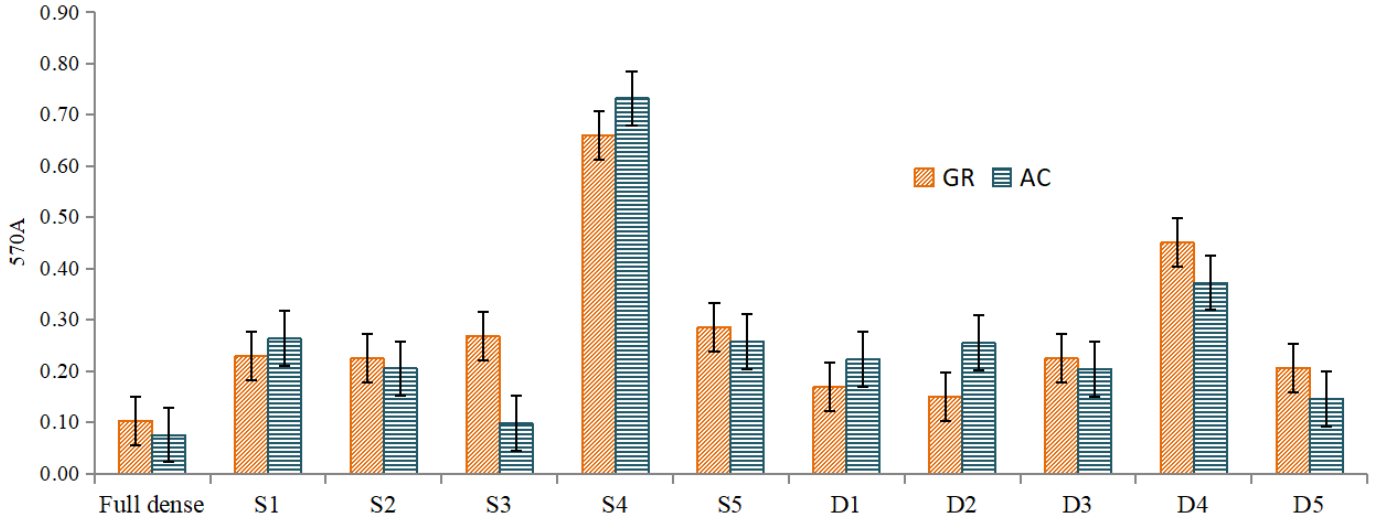

g. 9. Relationship of different sterilization techniques on cell viability of the metamaterials.

3.4. Effect of sterilization technique on CoCrMo metamaterials on-vitro

Implant materials as bone substitution that has intimate contact with bone need to be properly sterilized prior to the implantation. Basically, sterilization was considered for the final procedure during the manufacturing process due to physico-chemical properties of implant surface can change and give critical clinical impact later [95, 96]. Furthermore, sterilization is being applied as an essential step prior to biological testing such as *in vitro* and *in vivo* studies to enable the implant components free from viable microorganisms. This process can prevent the proliferation and accumulation of unwanted microorganism during biological studies [97]. In this work, autoclave and gamma ray irradiation were being selected due to cost and effectiveness. The autoclave technique offer cost effectiveness and efficacy. Previous study reported that autoclave caused a phase and surface characteristics changed because some biomaterials cannot withstand invasive moisture or high temperature above 100 °C [98]. Meanwhile, gamma irradiation is available to all microorganisms and this technique has an advantage of sterilizing without chemical or gases, high temperature and pressures. The ultimate goal for this work was to sterilize the metamaterials properly and without compromising the surface characteristics that can affect the interaction of components with surrounding chondrocytes cell in the cell culture process.

Fig. 9 shows the absorbance results of cell viability for each sterilization technique for gamma irradiated and autoclave components after being cultured for 14 days in the incubator. From the figure, the overall absorbance readings for gamma irradiated components were higher than autoclaved components. The biological, chemical and mechanical properties of implant materials are prone to change by different sterilization techniques. In this study, the gamma irradiated components could increase the formation of outermost molecular layer of CoCrMo metamaterials that resulted in the increase of surface wettability, chemistry and surface energy [99-101]. Thus, the surface wettability of gamma irradiated was enhanced without changing the surface roughness and suitable for cell attachment and cell proliferation in CoCrMo metamaterials. The metamaterials sterilized by autoclave had lost the characteristics increase of cell proliferation correlated to changed surface wettability and surface roughness. Thus, further study on significant effect and formation of the oxide layer that can enhance cell proliferation and differentiation should be considered in future work.

3.5. In-vitro biocompatibility of CoCrMo metamaterials

Biocompatibility of CoCrMo metamaterials fabricated by SLM was studied *in vitro* by using chondrocytes cell harvested from articular cartilage of an adult rabbit. From the biomaterials perspective, CoCrMo alloys have been routinely used in orthopaedic implants. In addition, *in vitro* biocompatibility studies to analyse the biological response towards the SLM-manufactured metamaterials made from CoCrMo are worth to be investigated. As can be seen from Fig. 9, the highest absorbance readings represent the highest cell viability (S4 and D4) after a selected time period. At day 14, the cellular activities were presumed at the optimum stage which involved cell-to-cell communication and cell-to-matrix interaction with regards to new cells formation. Hence, the viability of the cells in the 3D constructs of fabricated CoCrMo metamaterials was proven using SLM.

The graph illustrates that the in vitro cell viability shows the highest result for bigger pore size which was highly dependent on the pore shape. However, in this study, the stability and homogenous cell viability were found in the pore size (1.1 to 1.7 mm). Previously, Rumpler, et al. [102] found that the local growth rate of tissue formation was strongly influenced by the geometrical features of channels in cellular structures, where the pore curvature drives the effects and mechanical forced toward tissue regeneration. In this way, the angle of struts and larger surface area could rather promote and guide the tissue growth on stead of influencing the cell behaviour in a specific manner. For the full dense sample and metamaterials that possess smaller pore size, the absorbency intensity was found to be lower due to the inability of the cells to easily bridge the structure pore. Apart from that, the absorbency on full dense and smaller pore size metamaterials was lower.

Therefore, it was proven that produced metamaterials by SLM were not harmful to the cells which allow the cells to grow healthy and proliferate among them in the produced metamaterials. The results of biocompatibility analysis in this study were in line to the previous study on CoCrMo produced by AM techniques [33, 103] and commercial manufacturing process [104, 105] for orthopaedic implants applications.

3.6. SEM morphology of cellular response on CoCrMo metamaterials

At the microscopic level observation, the metamaterials offer an adequate substrate that was favourable to cell proliferation in the larger pore size component (2.1 mm and 1.5 m). Fig. 10 shows the SEM images of the highest cell viability of square and diamond pore shape with the formation of cell matrix attached to the metamaterials after day 21 culture. The proliferation cells in the well plate managed to adhere to each other and the metamaterials in dense were aggregated, which further allows the cells to synthesize the cartilage extracellular matrix (ECM) during the tissue formation process. Noticeably, ECM spread across the surface of the metamaterials into the inner surface and became confluent, but the cell could not cover the whole surface area after 21 days.

It was proven that both of the designed metamaterials have optimal benefits to cell growth, including its ability to differentiate initial tissue formation for integration between metamaterials. It was shown that the manufacturing process of SLM in this study did not contaminate the produced metamaterials. The in-vitro biocompatibility in this study demonstrated no cytotoxic effect and had the good agreement to the previous study [106-108]. The interconnected metamaterials encouraged the cell growth and proliferation in the metamaterials except for full dense configurations where most of the cells were gathered at the wells plate surface. Under SEM visualization for the cell response analysis, metamaterials were conducive for cell attachment and proliferation parallel to trabecular-like scaffolds as the reports from previous studies [109-111].

4. Conclusion

This study has investigated the selective laser melting (SLM) fabrication of CoCrMo square and diamond type metamaterials for orthopaedic implant application. Overall, the metamaterials were found to exhibit highly controlled geometrical parameters, particularly unit cell length, L_{cell} (1.5 to 2.5 mm) and strut size, Φ_S (0.4 to 0.6 mm) with porosity ranging from 44.8 % to 91% and pore size of 0.9 and 2.1 mm. The manufacturability of strut core, dimensional accuracy, density, mechanical properties, and biocompatibility of CoCrMo metamaterials have been systematically evaluated. The major findings of this research are described as follows:

- The SLM-manufactured CoCrMo metamaterials are in good geometrical agreement with the original CAD models. However, optical microscope observations revealed that numerous partially melted powder particles were attached to the strut surface, especially for the square type which can lead to higher strut size and smaller pore size compared to the original CAD models

- The manufacturability accuracy of strut size justified that the tested diamond unit cell type possesses higher potential in achieving the net shape compared to square unit cell, which further demonstrated maximum errors at the lateral part of the specimen of 3% and vertical part. This happens due to the capability of self-supported feature to reduce the overhang effect

- Higher energy density for the product of the process parameters can influence the density of the produced metamaterials

- Mechanicals stiffness of CoCrMo is comparable to human bone properties for orthopaedic use. It can be achieved when the tested elastic modulus of produced metamaterials are in the range of 0.45 GPa to 8.74 GPa and compressive strength of 10.77 MPa to 245.03 MPa. The component managed to exhibit the porosity of 44.8% to 91%. All specimens passed the toxicity test; however, the specimens with unit cell length of 2.5 mm and strut size 0.4 mm of both unit cell types showed the highest absorbance reading of cell viability

- Components that exhibit porosity 60% to 80% and pore sizes ranging 1.2 to 1.7 mm are best suited for orthopaedic implants due to their excellent mechanical strength and elastic modulus that are comparable to human bone properties, which is believed to offer better biological response for in vitro studies

Acknowledgements

The authors are grateful to the Ministry of Education Malaysia and Universiti Malaysia Pahang, Malaysia (www.ump.edu.my) for financial supports given under FRGS/1/2016/TK03/UMP/02/17 and PGRS1903164. The authors are indebted to Dipl-Ing. Muhammad Izuddin Abdul Hamid from Contraves Advanced Devices Sdn. Bhd. for SLM fabrication and constructive discussion. Furthermore,

the authors would like to express the gratitude to Mr. Muhammad Azri Ifwat Mohamed Amin for the assistance in-vitro laboratory experiment at Tissue Engineering Laboratory, Department of Biomedical, Kulliyah of Allied Health Sciences, IIUM.

Reference

[1] A. Sihvola, "Metamaterials in electromagnetics," *Metamaterials,* vol. 1, no. 1, pp. 2-11, 2007.

[2] E. Shamonina and L. Solymar, "Metamaterials: How the subject started," *Metamaterials,* vol. 1, no. 1, pp. 12-18, 2007.

[3] O. Acher, "Copper vs. iron: Microwave magnetism in the metamaterial age," *Journal of Magnetism and Magnetic Materials,* vol. 321, no. 14, pp. 2093-2101, 2009.

[4] E. G. Starodubtsev, "Characteristic properties of electromagnetic wave interaction with uniaxial absorbing metamaterials: A case of the near-zero axial parameter," *Metamaterials,* vol. 4, no. 1, pp. 32-43, 2010.

[5] B. Kante, A. Ourir, S. N. Burokur, F. Gadot, and A. de Lustrac, "Metamaterials for optical and radio communications," *Comptes Rendus Physique,* vol. 9, no. 1, pp. 31-40, 2008.

[6] O. Rybin, M. Raza, T. Nawaz, and T. Abbas, "Evaluation of layer properties of effective parameters of metallic rod metamaterials in GHz frequencies," *AEU - International Journal of Electronics and Communications,* vol. 63, no. 8, pp. 648-652, 2009.

[7] S. He, Y. Cui, Y. Ye, P. Zhang, and Y. Jin, "Optical nano-antennas and metamaterials," *Materials Today,* vol. 12, no. 12, pp. 16-24, 2009.

[8] A. Potts, A. Papakostas, D. M. Bagnall, and N. I. Zheludev, "Planar chiral meta-materials for optical applications," *Microelectronic Engineering,* vol. 73–74, pp. 367-371, 2004.

[9] J.-M. Lourtioz, "Photonic crystals and metamaterials," *Comptes Rendus Physique,* vol. 9, no. 1, pp. 4-15, 2008.

[10] M.-H. Lu, L. Feng, and Y.-F. Chen, "Phononic crystals and acoustic metamaterials," *Materials Today,* vol. 12, no. 12, pp. 34-42, 2009.

[11] R. Yang, Y. J. Xie, X. F. Li, and J. Jiang, "Slow wave propagation in nonradiative dielectric waveguides with bianisotropic split ring resonator metamaterials," *Infrared Physics & Technology,* vol. 51, no. 6, pp. 555-558, 2008.

[12] X. P. Zhao, Q. Zhao, L. Kang, J. Song, and Q. H. Fu, "Defect effect of split ring resonators in left-handed metamaterials," *Physics Letters A,* vol. 346, no. 1–3, pp. 87-91, 2005.

[13] Q. A. Naqvi and M. Abbas, "Fractional duality and metamaterials with negative permittivity and permeability," *Optics Communications,* vol. 227, no. 1–3, pp. 143-146, 2003.

[14] M. Maksimović and Z. Jakšić, "Modification of thermal radiation by periodical structures containing negative refractive index metamaterials," *Physics Letters A,* vol. 342, no. 5–6, pp. 497-503, 2005.

[15] N. C. Panoiu and R. M. Osgood Jr, "Numerical investigation of negative refractive index metamaterials at infrared and optical frequencies," *Optics Communications,* vol. 223, no. 4–6, pp. 331-337, 2003.

[16] S. Amin Yavari *et al.*, "Relationship between unit cell type and porosity and the fatigue behavior of selective laser melted meta-biomaterials," *Journal of the Mechanical Behavior of Biomedical Materials,* vol. 43, no. 0, pp. 91-100, 2015.

[17] M. S. Scholz *et al.*, "The use of composite materials in modern orthopaedic medicine and prosthetic devices: A review," *Composites Science and Technology,* vol. 71, no. 16, pp. 1791-1803, 2011.

[18] M. S. Taljanovic, M. D. Jones, J. T. Ruth, J. B. Benjamin, J. E. Sheppard, and T. B. Hunter, "Fracture Fixation," *RadioGraphics,* vol. 23, no. 6, pp. 1569-1590, 2003.

[19] N. J. Hallab and J. J. Jacobs, "Chapter II.5.6 - Orthopedic Applications," in *Biomaterials Science (Third Edition)*, B. D. R. S. H. J. S. E. Lemons, Ed.: Academic Press, 2013, pp. 841-882.

[20] P. M. Murray, "Prosthetic Replacement of the Proximal Interphalangeal Joint," *Hand Clinics,* vol. 22, no. 2, pp. 201-206, 2006.

[21] R. W. Molinari, "Dynamic stabilization of the lumbar spine," *Current Opinion in Orthopaedics,* vol. 18, no. 3, pp. 215-220, 2007.

[22] G. D. Schroeder, M. R. Murray, and W. K. Hsu, "A Review of Dynamic Stabilization in the Lumbar Spine," *Operative Techniques in Orthopaedics,* vol. 21, no. 3, pp. 235-239, 2011.

[23] C. E. Misch, *Dental implant prosthetics*. Elsevier Health Sciences, 2014.

[24] M. Figliuzzi, F. Mangano, and C. Mangano, "A novel root analogue dental implant using CT scan and CAD/CAM: selective laser melting technology," *International Journal of Oral and Maxillofacial Surgery,* vol. 41, no. 7, pp. 858-862, 2012.

[25] J. A. Disegi, "Titanium alloys for fracture fixation implants," *Injury,* vol. 31, Supplement 4, no. 0, pp. D14-D17, 2000.

[26] B. Nakayama *et al.*, "Reconstruction using a three-dimensional orbitozygomatic skeletal model of titanium mesh plate and soft-tissue free flap transfer following total maxillectomy," *Plastic and reconstructive surgery,* vol. 114, no. 3, pp. 631-639, 2004.

[27] S. M. Kurtz, E. Lau, K. Ong, K. Zhao, M. Kelly, and K. J. Bozic, "Future Young Patient Demand for Primary and Revision Joint Replacement: National Projections from 2010 to 2030," *Clinical Orthopaedics and Related Research,* vol. 467, no. 10, pp. 2606-2612, 2009.

[28] S. Kurtz, K. Ong, and E. Lau, "Projections of primary and revision hip and knee arthroplasty in the United States from 2005 to 2030. J Bone Jt Surg 89: 780," ed, 2007.

[29] K. Ren, A. Dusad, Y. Zhang, and D. Wang, "Therapeutic intervention for wear debris-induced aseptic implant loosening," *Acta Pharmaceutica Sinica B,* vol. 3, no. 2, pp. 76-85, 2013.

[30] K. J. Bozic and M. D. Ries, "Wear and osteolysis in total hip arthroplasty," in *Seminars in Arthroplasty*, 2005, vol. 16, no. 2, pp. 142-152: Elsevier.

[31] S. Landgraeber *et al.*, "Adiponectin attenuates osteolysis in aseptic loosening of total hip replacements," *Acta Biomaterialia,* vol. 10, no. 1, pp. 384-393, 1// 2014.

[32] L. E. Murr, S. M. Gaytan, E. Martinez, F. Medina, and R. B. Wicker, "Next generation orthopaedic implants by additive manufacturing using electron beam melting," *International journal of biomaterials,* vol. 2012, 2012.

[33] F. A. España, V. K. Balla, S. Bose, and A. Bandyopadhyay, "Design and fabrication of CoCrMo alloy based novel structures for load bearing implants using laser engineered net shaping," *Materials Science and Engineering: C,* vol. 30, no. 1, pp. 50-57, 2010.

[34] S. L. Sing, J. An, W. Y. Yeong, and F. E. Wiria, "Laser and electron‐beam powder‐bed additive manufacturing of metallic implants: A review on processes, materials and designs," *Journal of Orthopaedic Research,* vol. 34, no. 3, pp. 369-385, 2016.

[35] X. Wang *et al.*, "Topological design and additive manufacturing of porous metals for bone scaffolds and orthopaedic implants: A review," *Biomaterials,* vol. 83, pp. 127-141, 2016.

[36] S. M. Gaytan *et al.*, "Fabrication of barium titanate by binder jetting additive manufacturing technology," *Ceramics International,* vol. 41, no. 5, Part A, pp. 6610-6619, 6// 2015.

[37] J. Stampfl and M. Hatzenbichler, "Additive Manufacturing Technologies," in *CIRP Encyclopedia of Production Engineering*: Springer, 2014, pp. 20-27.

[38] A. A. Zadpoor and J. Malda, "Additive Manufacturing of Biomaterials, Tissues, and Organs," ed: Springer, 2017.

[39] L. Podshivalov, C. M. Gomes, A. Zocca, J. Guenster, P. Bar-Yoseph, and A. Fischer, "Design, Analysis and Additive Manufacturing of Porous Structures for Biocompatible Micro-Scale Scaffolds," *Procedia CIRP,* vol. 5, pp. 247-252, 2013.

[40] F. Bechmann, "Changing the future of additive manufacturing," *Metal Powder Report,* vol. 69, no. 3, pp. 37-40, 2014.

[41] F. Brenne, T. Niendorf, and H. J. Maier, "Additively manufactured cellular structures: Impact of microstructure and local strains on the monotonic and cyclic behavior under uniaxial and bending load," *Journal of Materials Processing Technology,* vol. 213, no. 9, pp. 1558-1564, 2013.

[42] G. Ryan, A. Pandit, and D. P. Apatsidis, "Fabrication methods of porous metals for use in orthopaedic applications," *Biomaterials,* vol. 27, no. 13, pp. 2651-2670, 2006.

[43] G. Campoli, M. S. Borleffs, S. Amin Yavari, R. Wauthle, H. Weinans, and A. A. Zadpoor, "Mechanical properties of open-cell metallic

biomaterials manufactured using additive manufacturing," *Materials & Design,* vol. 49, no. 0, pp. 957-965, 2013.
[44] J. Parthasarathy, B. Starly, S. Raman, and A. Christensen, "Mechanical evaluation of porous titanium (Ti6Al4V) structures with electron beam melting (EBM)," *Journal of the Mechanical Behavior of Biomedical Materials,* vol. 3, no. 3, pp. 249-259, 2010.
[45] S. Van Bael *et al.*, "The effect of pore geometry on the in vitro biological behavior of human periosteum-derived cells seeded on selective laser-melted Ti6Al4V bone scaffolds," *Acta Biomaterialia,* vol. 8, no. 7, pp. 2824-2834, 2012.
[46] X. B. Su, Y. Q. Yang, P. Yu, and J. F. Sun, "Development of porous medical implant scaffolds via laser additive manufacturing," *Transactions of Nonferrous Metals Society of China,* vol. 22, Supplement 1, no. 0, pp. s181-s187, 2012.
[47] S. Babaee, B. H. Jahromi, A. Ajdari, H. Nayeb-Hashemi, and A. Vaziri, "Mechanical properties of open-cell rhombic dodecahedron cellular structures," *Acta Materialia,* vol. 60, no. 6–7, pp. 2873-2885, 2012.
[48] M. G. Rashed, M. Ashraf, R. A. W. Mines, and P. J. Hazell, "Metallic microlattice materials: A current state of the art on manufacturing, mechanical properties and applications," *Materials & Design,* vol. 95, pp. 518-533, 2016.
[49] J. Parthasarathy, B. Starly, and S. Raman, "A design for the additive manufacture of functionally graded porous structures with tailored mechanical properties for biomedical applications," *Journal of Manufacturing Processes,* vol. 13, no. 2, pp. 160-170, 2011.
[50] F. Li, J. Li, G. Xu, G. Liu, H. Kou, and L. Zhou, "Fabrication, pore structure and compressive behavior of anisotropic porous titanium for human trabecular bone implant applications," *Journal of the Mechanical Behavior of Biomedical Materials,* vol. 46, no. 0, pp. 104-114, 2015.
[51] S. M. Ahmadi *et al.*, "Mechanical behavior of regular open-cell porous biomaterials made of diamond lattice unit cells," *Journal of the Mechanical Behavior of Biomedical Materials,* vol. 34, no. 0, pp. 106-115, 2014.
[52] L. Yang, O. Harrysson, H. West, and D. Cormier, "Mechanical properties of 3D re-entrant honeycomb auxetic structures realized via additive manufacturing," *International Journal of Solids and Structures,* 2015.
[53] N. Anisimova, M. Kiselevsky, I. Sukhorukova, N. Shvindina, and D. Shtansky, "Fabrication method, structure, mechanical, and biological properties of decellularized extracellular matrix for replacement of wide bone tissue defects," *Journal of the Mechanical Behavior of Biomedical Materials,* 2015.
[54] S. P. Lake, S. Ray, A. M. Zihni, D. M. Thompson Jr, J. Gluckstein, and C. R. Deeken, "Pore size and pore shape – but not mesh density – alter the mechanical strength of tissue ingrowth and host tissue response to synthetic mesh materials in a porcine model of ventral hernia repair," *Journal of the Mechanical Behavior of Biomedical Materials,* vol. 42, no. 0, pp. 186-197, 2015.
[55] J. Van der Stok *et al.*, "Selective laser melting ‐ produced porous titanium scaffolds regenerate bone in critical size cortical bone defects," *Journal of Orthopaedic Research,* vol. 31, no. 5, pp. 792-799, 2013.
[56] N. Taniguchi *et al.*, "Effect of pore size on bone ingrowth into porous titanium implants fabricated by additive manufacturing: An in vivo experiment," *Materials Science and Engineering: C,* vol. 59, pp. 690-701, 2016.
[57] S. Arabnejad, R. Burnett Johnston, J. A. Pura, B. Singh, M. Tanzer, and D. Pasini, "High-strength porous biomaterials for bone replacement: A strategy to assess the interplay between cell morphology, mechanical properties, bone ingrowth and manufacturing constraints," *Acta Biomaterialia,* vol. 30, pp. 345-356, 2016/01/15/ 2016.
[58] D. Hara *et al.*, "Bone bonding strength of diamond-structured porous titanium-alloy implants manufactured using the electron beam-melting technique," *Materials Science and Engineering: C,* vol. 59, pp. 1047-1052, 2016.
[59] T. Douglas *et al.*, "Rapid Prototyping: Porous Titanium Alloy Scaffolds Produced by Selective Laser Melting (SLM) for Bone Tissue Engineering," in *TISSUE ENGINEERING PART A*, 2009, vol. 15, no. 5, pp. O7-O8: MARY ANN LIEBERT INC 140 HUGUENOT STREET, 3RD FL, NEW ROCHELLE, NY 10801 USA.
[60] M. Dourandish, D. Godlinski, A. Simchi, and V. Firouzdor, "Sintering of biocompatible P/M Co–Cr–Mo alloy (F-75) for fabrication of porosity-graded composite structures," *Materials Science and Engineering: A,* vol. 472, no. 1, pp. 338-346, 2008/01/15/ 2008.
[61] I. 13314:2011, "ISO 13314: 2011 (E)(2011) Mechanical testing of metals—ductility testing—compression test for porous and cellular metals," *Ref Number ISO,* vol. 13314, no. 13314, pp. 1-7.
[62] I. S. Organization, "ISO 10993 ‐ 5: 2009. Biological evaluation of medical devices ‐ Part 5: Tests for in vitro cytotoxicity," 2009.
[63] K. A. Mumtaz, P. Erasenthiran, and N. Hopkinson, "High density selective laser melting of Waspaloy®," *Journal of materials processing technology,* vol. 195, no. 1, pp. 77-87, 2008.
[64] M. Xia, D. Gu, G. Yu, D. Dai, H. Chen, and Q. Shi, "Influence of hatch spacing on heat and mass transfer, thermodynamics and laser processability during additive manufacturing of Inconel 718 alloy," *International Journal of Machine Tools and Manufacture,* vol. 109, pp. 147-157, 2016.
[65] C. Yan, L. Hao, A. Hussein, and P. Young, "Ti–6Al–4V triply periodic minimal surface structures for bone implants fabricated via selective laser melting," *Journal of the Mechanical Behavior of Biomedical Materials,* vol. 51, pp. 61-73, 2015.
[66] C. Yan, L. Hao, A. Hussein, and D. Raymont, "Evaluations of cellular lattice structures manufactured using selective laser melting," *International Journal of Machine Tools and Manufacture,* vol. 62, no. 0, pp. 32-38, 2012.
[67] C. Yan, L. Hao, A. Hussein, S. L. Bubb, P. Young, and D. Raymont, "Evaluation of light-weight AlSi10Mg periodic cellular lattice structures fabricated via direct metal laser sintering," *Journal of Materials Processing Technology,* vol. 214, no. 4, pp. 856-864, 2014.
[68] J. P. Kruth, S. Kumar, and J. Van Vaerenbergh, "Study of laser-sinterability of ferro-based powders," *Rapid Prototyping Journal,* vol. 11, no. 5, pp. 287-292, 2005.
[69] G. Pyka, G. Kerckhofs, J. Schrooten, and M. Wevers, "The effect of spatial micro-CT image resolution and surface complexity on the morphological 3D analysis of open porous structures," *Materials Characterization,* vol. 87, no. 0, pp. 104-115, 1// 2014.
[70] D. N. Silva, M. G. De Oliveira, E. Meurer, M. I. Meurer, J. V. L. da Silva, and A. Santa-Bárbara, "Dimensional error in selective laser sintering and 3D-printing of models for craniomaxillary anatomy reconstruction," *Journal of cranio-maxillofacial surgery,* vol. 36, no. 8, pp. 443-449, 2008.
[71] X. Zhou, X. Liu, D. Zhang, Z. Shen, and W. Liu, "Balling phenomena in selective laser melted tungsten," *Journal of Materials Processing Technology,* vol. 222, no. 0, pp. 33-42, 8// 2015.
[72]Z. A. Mat Taib, W. S. Wan Harun, S. A. Che Ghani, M. F. F. Ab Rashid, M. A. Omar, and H. Ramli, "Dimensional Accuracy Study of Open Cellular Structure CoCrMo Alloy Fabricated by Selective Laser Melting Process," in *Advanced Materials Research*, 2016, vol. 1133, pp. 280-284: Trans Tech Publ.
[73] H. Lei *et al.*, "Evaluation of compressive properties of SLM-fabricated multi-layer lattice structures by experimental test and μ-CT-based finite element analysis," *Materials & Design,* vol. 169, p. 107685, 2019.
[74] M. Dallago, F. Zanini, S. Carmignato, D. Pasini, and M. Benedetti, "Effect of the geometrical defectiveness on the mechanical properties of SLM biomedical Ti6Al4V lattices," *Procedia Structural Integrity,* vol. 13, pp. 161-167, 2018/01/01/ 2018.
[75] A. Lerebours, P. Vigneron, S. Bouvier, A. Rassineux, M. Bigerelle, and C. Egles, "Additive manufacturing process creates local surface roughness modifications leading to variation in cell adhesion on multifaceted TiAl6V4 samples," *Bioprinting,* vol. 16, p. e00054, 2019/12/01/ 2019.
[76] C. Chen *et al.*, "3D printed porous Ti6Al4V cage: Effects of additive angle on surface properties and biocompatibility; bone ingrowth in Beagle tibia model," *Materials & Design,* vol. 175, p. 107824, 2019/08/05/ 2019.
[77] C. Yan, L. Hao, A. Hussein, P. Young, and D. Raymont, "Advanced lightweight 316L stainless steel cellular lattice structures fabricated via selective laser melting," *Materials & Design,* vol. 55, no. 0, pp. 533-541, 2014.
[78] S. Van Bael, G. Kerckhofs, M. Moesen, G. Pyka, J. Schrooten, and J. P. Kruth, "Micro-CT-based improvement of geometrical and

mechanical controllability of selective laser melted Ti6Al4V porous structures," *Materials Science and Engineering: A,* vol. 528, no. 24, pp. 7423-7431, 2011/09/15/ 2011.

[79] L. Mullen, R. C. Stamp, W. K. Brooks, E. Jones, and C. J. Sutcliffe, "Selective Laser Melting: A regular unit cell approach for the manufacture of porous, titanium, bone in‐growth constructs, suitable for orthopedic applications," *Journal of Biomedical Materials Research Part B: Applied Biomaterials,* vol. 89, no. 2, pp. 325-334, 2009.

[80] M. Santorinaios, W. Brooks, C. Sutcliffe, and R. Mines, "Crush behaviour of open cellular lattice structures manufactured using selective laser melting," *WIT Transactions on the Built Environment,* vol. 85, 2006.

[81] C. Domínguez-Trujillo *et al.*, "Improvement of the balance between a reduced stress shielding and bone ingrowth by bioactive coatings onto porous titanium substrates," *Surface and Coatings Technology,* vol. 338, pp. 32-37, 2018/03/25/ 2018.

[82] J. Li, J. A. Jansen, X. F. Walboomers, and J. J. J. P. van den Beucken, "Mechanical aspects of dental implants and osseointegration: A narrative review," *Journal of the Mechanical Behavior of Biomedical Materials,* vol. 103, p. 103574, 2020/03/01/ 2020.

[83] L. Xiao *et al.*, "Mechanical properties of open-cell rhombic dodecahedron titanium alloy lattice structure manufactured using electron beam melting under dynamic loading," *International Journal of Impact Engineering,* vol. 100, pp. 75-89, 2017.

[84] Y. J. Liu *et al.*, "Microstructure, defects and mechanical behavior of beta-type titanium porous structures manufactured by electron beam melting and selective laser melting," *Acta Materialia,* vol. 113, pp. 56-67, 2016.

[85] I. Maskery *et al.*, "A mechanical property evaluation of graded density Al-Si10-Mg lattice structures manufactured by selective laser melting," *Materials Science and Engineering: A,* vol. 670, pp. 264-274, 2016.

[86] Y. H. An and R. A. Draughn, *Mechanical testing of bone and the bone-implant interface*. CRC press, 1999.

[87] N. A. Malek, S. Mohamed, S. C. Ghani, and W. W. Harun, "Critical evaluation on structural stiffness of porous cellular structure of cobalt chromium alloy," in *IOP Conference Series: Materials Science and Engineering*, 2015, vol. 100, no. 1, p. 012019: IOP Publishing.

[88] R. Hasan, R. A. Mines, E. Shen, S. Tsopanos, and W. Cantwell, "Comparison on compressive behaviour of aluminium honeycomb and titanium alloy micro lattice blocks," in *Key Engineering Materials*, 2011, vol. 462, pp. 213-218: Trans Tech Publ.

[89] I. Maskery *et al.*, "A mechanical property evaluation of graded density Al-Si10-Mg lattice structures manufactured by selective laser melting," *Materials Science and Engineering: A,* vol. 670, pp. 264-274, 2016.

[90] C. Qiu *et al.*, "Influence of processing conditions on strut structure and compressive properties of cellular lattice structures fabricated by selective laser melting," *Materials Science and Engineering: A,* vol. 628, pp. 188-197, 2015.

[91] V. Weißmann, R. Bader, H. Hansmann, and N. Laufer, "Influence of the structural orientation on the mechanical properties of selective laser melted Ti6Al4V open-porous scaffolds," *Materials & Design,* vol. 95, pp. 188-197, 2016.

[92] P. Onck, E. Andrews, and L. Gibson, "Size effects in ductile cellular solids. Part I: modeling," *International Journal of Mechanical Sciences,* vol. 43, no. 3, pp. 681-699, 2001.

[93] E. Andrews, G. Gioux, P. Onck, and L. Gibson, "Size effects in ductile cellular solids. Part II: experimental results," *International Journal of Mechanical Sciences,* vol. 43, no. 3, pp. 701-713, 2001.

[94] A. Yánez, A. Herrera, O. Martel, D. Monopoli, and H. Afonso, "Compressive behaviour of gyroid lattice structures for human cancellous bone implant applications," *Materials Science and Engineering: C,* vol. 68, pp. 445-448, 2016.

[95] N. P. Tipnis and D. J. Burgess, "Sterilization of implantable polymer-based medical devices: A review," *International Journal of Pharmaceutics,* vol. 544, no. 2, pp. 455-460, 2018/06/15/ 2018.

[96] M. Ahmed, G. Punshon, A. Darbyshire, and A. M. Seifalian, "Effects of sterilization treatments on bulk and surface properties of nanocomposite biomaterials," *Journal of Biomedical Materials Research Part B: Applied Biomaterials,* vol. 101, no. 7, pp. 1182-1190, 2013.

[97] W. A. Rutala and D. J. Weber, "Disinfection, sterilization, and antisepsis: An overview," *American Journal of Infection Control,* vol. 44, no. 5, Supplement, pp. e1-e6, 2016/05/02/ 2016.

[98] T. Kuwahara, "Reduction in Energy Consumption Using Fuel Cells in Nonthermal Plasma-Based Water Sterilization by Bubbling Ozone," *IEEE Transactions on Industry Applications,* vol. 54, no. 6, pp. 6414-6421, 2018.

[99] J. H. Park *et al.*, "Effect of cleaning and sterilization on titanium implant surface properties and cellular response," *Acta Biomaterialia,* vol. 8, no. 5, pp. 1966-1975, 2012/05/01/ 2012.

[100] A. Han, J. K. H. Tsoi, J. P. Matinlinna, Y. Zhang, and Z. Chen, "Effects of different sterilization methods on surface characteristics and biofilm formation on zirconia in vitro," *Dental Materials,* vol. 34, no. 2, pp. 272-281, 2018/02/01/ 2018.

[101] K. Odelius, P. Plikk, and A.-C. Albertsson, "The influence of composition of porous copolyester scaffolds on reactions induced by irradiation sterilization," *Biomaterials,* vol. 29, no. 2, pp. 129-140, 2008/01/01/ 2008.

[102] M. Rumpler, A. Woesz, J. W. Dunlop, J. T. van Dongen, and P. Fratzl, "The effect of geometry on three-dimensional tissue growth," *Journal of the Royal Society Interface,* vol. 5, no. 27, pp. 1173-1180, 2008.

[103] B. Vamsi Krishna, W. Xue, S. Bose, and A. Bandyopadhyay, "Functionally graded Co–Cr–Mo coating on Ti–6Al–4V alloy structures," *Acta Biomaterialia,* vol. 4, no. 3, pp. 697-706, 2008.

[104] M. Andrei *et al.*, "Electrochemical comparison and biological performance of a new CoCrNbMoZr alloy with commercial CoCrMo alloy," *Materials Science and Engineering: C,* vol. 59, pp. 346-355, 2016.

[105] L. Qin, Q. Zeng, W. Wang, Y. Zhang, and G. Dong, "Response of MC3T3-E1 osteoblast cells to the microenvironment produced on Co–Cr–Mo alloy using laser surface texturing," *Journal of Materials Science,* vol. 49, no. 6, pp. 2662-2671, 2014.

[106] A. Bandyopadhyay, A. Shivaram, M. Isik, J. D. Avila, W. S. Dernell, and S. Bose, "Additively manufactured calcium phosphate reinforced CoCrMo alloy: Bio-tribological and biocompatibility evaluation for load-bearing implants," *Additive Manufacturing,* vol. 28, pp. 312-324, 2019/08/01/ 2019.

[107] D. de Castro Girão *et al.*, "An assessment of biomedical CoCrMo alloy fabricated by direct metal laser sintering technique for implant applications," *Materials Science and Engineering: C,* vol. 107, p. 110305, 2020/02/01/ 2020.

[108] Y. S. Hedberg, B. Qian, Z. Shen, S. Virtanen, and I. Odnevall Wallinder, "In vitro biocompatibility of CoCrMo dental alloys fabricated by selective laser melting," *Dental Materials,* vol. 30, no. 5, pp. 525-534, 2014/05/01/ 2014.

[109] H. Liang *et al.*, "Trabecular-like Ti-6Al-4V scaffolds for orthopedic: fabrication by selective laser melting and in vitro biocompatibility," *Journal of Materials Science & Technology,* vol. 35, no. 7, pp. 1284-1297, 2019/07/01/ 2019.

[110] Y. Li *et al.*, "Novel β-Ti35Zr28Nb alloy scaffolds manufactured using selective laser melting for bone implant applications," *Acta Biomaterialia,* vol. 87, pp. 273-284, 2019/03/15/ 2019.

[111] W. Xu *et al.*, "Novel porous Ti35Zr28Nb scaffolds fabricated by powder metallurgy with excellent osteointegration ability for bone-tissue engineering applications," *Materials Science and Engineering: C,* vol. 105, p. 110015, 2019/12/01/ 2019.